

PRODUCTION OF AMORPHOUS SILICA FROM RICE HUSK IN FLUIDISED
BED SYSTEM

NGO SAIK PENG

A thesis submitted in fulfilment of the
requirements for the award of the degree of
Doctor of Philosophy

Faculty of Chemical Engineering and Natural Resources Engineering
Universiti Teknologi Malaysia

FEBRUARY 2006

ACKNOWLEDGEMENT

I would like to express my most sincere gratitude and appreciation to my supervisor, Assoc. Prof. Dr Mohd Rozainee bin Taib for his guidance and supervision of this research works. Without his guidance, I believe this research would not have been completed.

I am also grateful to my fellow research partners, Mr Tan Kean Giap, Mr Anwar Johari, Mr Arshad Adam Salema, Mr Wan Ahmad Muhandi bin Wan Muhammad, Mr Lim Sin Yang, Mr Simon Looi Yat Seong, Mr Chong Yee Hwang and Ms Wong Cheng Teng for their valuable ideas, friendship and assistance. I am equally grateful to the Research Assistants involved in my research especially Mr Guee Boon Chye, whose assistance facilitated my experimental works.

My special thanks go to the School of Graduate Studies (SPS) who supported me financially through the UTM Fellowship Award. Lastly but certainly not the least, I am indebted to my parents for their endless support throughout the length of my study.

ABSTRACT

Conventional methods for the preparation of amorphous silica (SiO_2) are very energy-intensive and expensive. Amorphous silica has wide industrial applications, with annual world consumption in the excess of 1 million tonnes valued at RM4,500 per tonne. Rice husk ash contains amorphous silica in the excess of 95 wt%. Thermal treatment of rice husk is deemed the most economical method to recover this amorphous silica from the readily available rice husk (approximately 0.5 million tonnes per annum in Malaysia). Hence, the purpose of this research was to recover amorphous silica from rice husk through thermal treatment in fluidised bed system. Experimental works were conducted in fluidised bed combustor systems to determine the optimum mixing parameters (sand size, fluidising velocity, static bed height) and combustion parameters (temperature, air supply, rice husk moisture content, feeding design) to produce amorphous, carbon-free silica from rice husk. The fly and bottom ashes were analysed for their residual carbon contents and silica structures through loss on ignition (LOI) tests and X-Ray Diffraction (XRD) analyses, respectively. Computational fluid dynamics (CFD) modelling using FLUENT was also conducted to optimise the fluidised bed design and to overcome problems encountered in experimental works. Experimental results showed that amorphous, siliceous ash with residual carbon content of down to 1.0 wt% could be obtained by burning water-washed rice husk that was free from alkali metal compounds (potassium oxide and sodium oxide). The short freeboard height of the experimental fluidised bed resulted in the incomplete oxidation of carbon and sand contamination in the ash. Modelling results showed that both problems could be overcome by increasing the height of the fluidised bed to 5000mm. In addition, the induction of swirling flows at the freeboard region was found to be beneficial in increasing the residence time of ash in the combustor, leading to higher carbon burnout.

ABSTRAK

Penyediaan silika amorfus (SiO_2) secara konvensional menggunakan banyak tenaga dan sangat mahal. Silika amorfus mempunyai penggunaan meluas di industri, dengan kadar penggunaannya di seluruh dunia melebihi 1 juta tan setahun dinilaikan pada RM4,500 per tan. Abu sekam padi mengandungi silika amorfus melebihi 95%. Rawatan haba ke atas sekam padi (dihasilkan pada kira-kira 0.5 juta tan setahun di Malaysia) adalah kaedah paling ekonomik untuk memperolehi silika amorfus. Oleh itu, matlamat penyelidikan ini adalah untuk mendapatkan silika amorfus daripada sekam padi melalui rawatan haba dalam lapisan terbendalir. Kerja eksperimen dilaksanakan dalam pembakar lapisan terbendalir untuk menentukan parameter percampuran (saiz pasir, halaju perbendaliran, ketinggian lapisan terbendalir) dan parameter pembakaran (suhu, bekalan udara, kelembapan sekam padi, rekabentuk sistem penyuapan) optimum bagi menghasilkan silika amorfus dan bebas karbon daripada sekam padi. Abu terbang dan abu bawahan dianalisis untuk menentukan baki karbon dan struktur silika masing-masing melalui analisis kehilangan jisim dan analisis belauan sinar-x. Permodelan pengiraan dinamik bendalir menggunakan kod program FLUENT juga dilaksanakan untuk pengoptimuman rekabentuk pembakar serta mengatasi masalah operasi semasa kerja eksperimen. Keputusan eksperimen menunjukkan abu sekam padi amorfus dengan kandungan karbon sisa serendah 1.0% dapat diperolehi dengan membakar sekam padi yang telah dibasuh dengan air (bebas dari sebatian logam alkali iaitu kalium oksida dan natrium oksida). Ketinggian pembakar yang tidak mencukupi menyebabkan pengoksidaan karbon tidak lengkap serta pencemaran pasir dalam abu terbang. Keputusan permodelan komputer menunjukkan masalah ini dapat diatasi dengan menambahkan ketinggian pembakar ke 5000mm. Penghasilan aliran pusaran di bahagian atas pembakar juga didapati berfaedah untuk meningkatkan masa mastautin abu di dalam pembakar, dan seterusnya menyebabkan kadar pengoksidaan karbon yang lebih tinggi.

TABLE OF CONTENTS

CHAPTER	TITLE	PAGE
	TITLE PAGE	i
	DECLARATION	ii
	ACKNOWLEDGEMENT	iii
	ABSTRACT	iv
	ABSTRAK	v
	TABLE OF CONTENTS	vi
	LIST OF TABLES	xi
	LIST OF FIGURES	xxi
	LIST OF PLATES	xxxii
	LIST OF SYMBOLS	xxxiv
	LIST OF APPENDICES	xl
1	INTRODUCTION	1
1.1	Introduction	1
1.2	Benefits of Research	2
1.2.1	Amorphous Silica	2
1.2.2	Rice Husk as Silica Source	4
1.2.3	Market Review for Amorphous Silica from Rice Husk Ash	8
1.2.4	Evaluation of Available Technologies for Production of Amorphous Silica from Rice Husk	11
1.2.5	Fluidised Bed as Selected Technology	16

1.2.6	Types of Fluidised Bed	19
1.3	Objectives of Research	21
1.4	Scopes of Research	22
1.5	Expected Results	23
1.6	Layout of the Thesis	24
2	LITERATURE REVIEW	26
2.1	Research History on Thermal Treatment of Rice Husk in Fluidised Bed	26
2.2	Effects of Fluidisation Parameters on the Mixing Characteristics of Rice Husk in Fluidised Bed	28
2.2.1	Fluidising Velocity	29
2.2.2	Sand Size	31
2.2.3	Static Bed Height	33
2.3	Effects of Operating Parameters on the Combustion Efficiency of Rice Husk in Fluidised Bed	37
2.3.1	Time	37
2.3.2	Temperature	39
2.3.3	Presence of Impurities in Rice Husk	51
2.3.4	Air Supply	57
2.3.5	Moisture Content of Rice Husk	60
2.4	Effects of Fluidised Bed Design on the Combustion Efficiency of Rice Husk in Fluidised Bed	61
2.4.1	Freeboard Height	61
2.4.2	Feeding Design and Position of Feed Entry	63
3	METHODOLOGY	67
3.1	Introduction	67
3.2	Research Materials	67

3.3	Experimental Techniques	75
3.3.1	Thermal Treatment in Muffle Furnace	75
3.3.2	Fluidisation Study in 80-mm Inner Diameter Fluidised Bed Column	76
3.3.3	Combustion Study in 80-mm Inner Diameter Fluidised Bed Combustor	80
3.3.4	Combustion Study in 210-mm Inner Diameter Fluidised Bed Combustor	83
3.4	Analytical Techniques	90
3.4.1	Determination Silica Structure and Presence of Contaminants in Rice Husk Ash through X-Ray Diffraction (XRD) Analysis	90
3.4.2	Determination of Residual Carbon Content in Rice Husk Ash through Loss on Ignition (LOI) Test	90
3.4.3	Determination of Particle Size Distribution of Rice Husk Ash through Sieve Analysis	91
3.4.4	Determination of Oxygen Level in Combustion Gas	92
3.5	Modelling Technique through Computational Fluid Dynamics (CFD) Code of FLUENT	92
3.5.1	Governing Equations	93
3.5.2	Numerical Solutions	106
4	RESULTS AND DISCUSSIONS ON COMBUSTION OF RICE HUSK IN FLUIDISED BED TO PRODUCE AMORPHOUS SILICA	114
4.1	Basic Combustion Characteristics of Rice Husk	114
4.2	Effect of Temperature and Residence Time on the Formation of Silica Crystals in Rice Husk Ash	119

4.3	Effects of Fluidisation Parameters on the Mixing of Rice Husk in Fluidised Bed	130
4.3.1	Sand Size	132
4.3.2	Fluidising Velocity (U_{mf} Number)	135
4.3.3	Static Bed Height	137
4.4	Effect of Fluidisation Parameters on the Mixing of Rice Husk in Fluidised Bed during Combustion Process	139
4.4.1	Sand Size	139
4.4.2	Fluidising Velocity	150
4.5	Effect of Mixing Parameters on the Combustion Efficiency of Rice Husk in Fluidised Bed	153
4.5.1	Fluidising Velocity	153
4.5.2	Static Bed Height	164
4.6	Effect of Temperature on the Combustion Efficiency of Rice Husk in Fluidised Bed	178
4.6.1	Bed Temperature	178
4.6.2	Freeboard Temperature	181
4.6.3	Heat Loss	193
4.7	Effect of Washing of Rice Husk on Its Combustion Efficiency in Fluidised Bed	201
4.7.1	Determination of Pretreatment Method for Rice Husk	201
4.7.2	Effect of Alkali Metals Removal in Rice Husk on Its Combustion Efficiency in Fluidised Bed	205
	4.7.2.1 Primary Stage Combustion	205
	4.7.2.2 Secondary Stage Combustion	209
4.8	Effect of Air Supply on the Combustion Efficiency of Rice Husk in Fluidised Bed	220
4.8.1	Primary Air Factor	220
4.8.2	Primary-to-Secondary Air Ratio	227
4.8.3	Pneumatic Air Feeding Velocity	232

4.9	Effect of Moisture Content in Rice Husk on Its Combustion Efficiency in Fluidised Bed	241
4.10	Effect of Feeding Design on the Combustion Efficiency of Rice Husk in Fluidised Bed	246
4.10.1	Vortex Feeding	246
4.10.2	Vortex Feeding with Higher Fluidising Velocity	263
4.11	Summary of Findings	273
5	RESULTS AND DISCUSSIONS ON IMPROVEMENT IN DESIGN AND OPERATION OF THE FLUIDISED BED THROUGH CFD MODELLING	277
5.1	Increase in Fluidised Bed Freeboard Height	277
5.2	Improvement of Feeding Conditions	284
5.2.1	Feeding Velocity	284
5.2.2	Vortex Feeding	292
5.3	Summary of Findings	310
6	CONCLUSIONS AND RECOMMENDATIONS	313
6.1	Conclusions	313
6.2	Recommendations for Future Study	323
	REFERENCES	325

LIST OF TABLES

TABLE	TITLE	PAGE
Table 1-1:	Market prices for amorphous rice husk ash for use in cement industry	10
Table 1-2:	Existing methods and technologies for preparation of amorphous silica from rice husk	12
Table 1-3:	Performance of existing thermal treatment technologies in producing low carbon content rice husk ash	18
Table 2-1:	Properties of sewage sludge and rice husk (wt% dry basis)	30
Table 2-2:	Sand size and corresponding fluidisation velocity reported in literature for combustion of rice husk in fluidised bed	31
Table 2-3:	Minimum fluidising velocity of sand of various size ranges	33
Table 2-4:	Static bed height used for the combustion of rice husk as reported in existing literatures	34
Table 2-5:	Temperature limits reported in various literatures for the onset of crystallisation of silica in rice husk ash	43
Table 2-6:	Chemical properties of wheat straw and rice husk	54
Table 2-7:	Optimum air factor reported in literature (as reviewed by Natarajan et al., 1998a) for combustion of rice husk in fluidised bed	57

Table 2-8:	Different rice husk feeding arrangements reported in literature	64
Table 3-1:	Chemical properties of rice husk	68
Table 3-2:	List and identifications of combustion parameters investigated in the 210-mm inner diameter fluidised bed combustor	89
Table 3-3:	Diffraction peaks of crystalline silica	90
Table 3-4:	Properties of particles used in modelling the effect of feeding method on rice husk combustion in the 210-mm inner diameter fluidised bed combustor	113
Table 4-1:	Real-time tracking of combustion of a batch (4 g) of water-washed rice husk particles in the muffle furnace (650 – 750°C)	118
Table 4-2:	Effect of temperature and residence time on the formation of black char particles during thermal treatment of raw rice husk in the muffle furnace	122
Table 4-3:	Effect of temperature and residence time on the formation of black char particles during thermal treatment of water-washed rice husk* in the muffle furnace	123
Table 4-4:	Effect of temperature and residence time on the formation of black char particles during thermal treatment of water-washed rice husk* (submerged particles) in the muffle furnace	124
Table 4-5:	Effect of temperature and residence time on the formation of black char particles during thermal treatment of water-washed rice husk* (floating particles) in the muffle furnace	125
Table 4-6:	Diffractograms of rice husk ash samples from thermal treatment of raw rice husk in the muffle furnace at different temperatures and residence times	127
Table 4-7:	Diffractograms of rice husk ash samples from thermal treatment of water-washed rice husk* in	

	the muffle furnace at different temperatures and residence times	128
Table 4-8:	Diffractograms of rice husk ash samples from thermal treatment of water-washed rice husk in the muffle furnace at 900°C for different residence times	129
Table 4-9:	Fluidisation properties of rice husk, rice husk char, rice husk ash and silica sand samples	131
Table 4-10:	Screening of commercial silica sand* size for experimental study of rice husk combustion in fluidised bed combustor systems	133
Table 4-11:	Mixing behaviours of rice husk in the 80-mm inner diameter fluidised bed column at different fluidising velocities (sand size = 250 – 595 μm , static bed height = 0.5 D_c , mass fraction of rice husk in sand bed = 10 wt%)	136
Table 4-12:	Mixing behaviours of rice husk in the 80-mm inner diameter fluidised bed column at different static bed heights (sand size = 250 – 595 μm , fluidising velocity = 4 U_{mf} , mass fraction of rice husk in sand bed = 10 wt%)	138
Table 4-13:	Fly ash samples from the combustion of rice husk in the 80-mm inner diameter fluidised bed combustor with a bed of 595 – 841 μm sand (fluidising velocity = 3 – 5 U_{mf} , static bed height = 0.5 D_c , primary air factor \approx 1.0)	140
Table 4-14:	Ash samples from the combustion of rice husk in the 80-mm inner diameter fluidised bed combustor with a bed of 250 – 595 μm sand (fluidising velocity = 3 – 5 U_{mf} , static bed height = 0.5 D_c , primary air factor \approx 1.0)	145
Table 4-15:	Ash samples from the combustion of rice husk in the 80-mm inner diameter fluidised bed combustor	

	at different fluidising velocities (sand size = 250 – 595 μm , static bed height = 0.5 D_c , primary air factor ≈ 1.0)	151
Table 4-16:	Diffraction patterns of fly ash samples from the combustion of rice husk in the 210-mm inner diameter fluidised bed at different fluidising velocities (sand size = 250 – 595 μm , static bed height = 0.5 D_c , primary air factor ≈ 1.0)	157
Table 4-17:	Products and diffraction patterns of fly ash sample after sand de-contamination stage	158
Table 4-18:	Ash samples from the combustion of rice husk in the 210-mm inner diameter fluidised bed combustor at different fluidising velocities (sand size = 250 – 595 μm , static bed height = 0.5 D_c , primary air factor ≈ 1.0)	161
Table 4-19:	Diffraction patterns of fly ash samples from the combustion of rice husk in the 210-mm inner diameter fluidised bed at different static bed heights (sand size = 250 – 595 μm , fluidising velocity $\approx 3 U_{mf}$, primary air factor ≈ 1.0)	174
Table 4-20:	Fly ash samples from the combustion of rice husk in the 210-mm inner diameter fluidised bed at different static bed heights (sand size = 250 – 595 μm , fluidising velocity $\approx 3 U_{mf}$, primary air factor ≈ 1.0)	177
Table 4-21:	Diffraction patterns of fly and bottom ashes from the combustion of rice husk in the 80-mm inner diameter fluidised bed at different bed temperatures (sand size = 250 – 595 μm , static bed height = 0.5 D_c , fluidising velocity $\approx 4 U_{mf}$, primary air factor ≈ 1.0)	179
Table 4-22:	Diffraction patterns of ash samples from the combustion of rice husk in the 210-mm inner	

	diameter fluidised bed combustor at different freeboard temperatures (sand size = 250 – 595 μm , static bed height = 0.5 D_c , fluidising velocity = 4 – 5 U_{mf} , primary air factor ≈ 1.0 , oxygen level in cyclone ≥ 6 vol%)	188
Table 4-23:	Ash samples from the combustion of rice husk in the 210-mm inner diameter fluidised bed at different freeboard temperatures (sand size = 250 – 595 μm , static bed height = 0.5 D_c , fluidising velocity = 4 – 5 U_{mf} , primary air factor ≈ 1.0 , oxygen level in cyclone ≥ 6 vol%)	192
Table 4-24:	Diffractiongrams of fly ash samples from the combustion of rice husk in the non-insulated and insulated 210-mm inner diameter fluidised bed combustors (sand size = 250 – 595 μm , static bed height = 0.5 D_c , fluidising velocity $\approx 3 U_{mf}$, primary air factor ≈ 1.5)	199
Table 4-25:	Ash samples from thermal treatment of raw, water-washed and acid-leached rice husk	204
Table 4-26:	Effect of alkali metals removal from rice husk on the bed temperatures during combustion of rice husk in the 210-mm inner diameter fluidised bed (primary stage combustion) (sand size = 250 – 595 μm , static bed height = 0.5 D_c , fluidising velocity $\approx 3 U_{mf}$, primary air factor ≈ 1.2)	206
Table 4-27:	Physical appearances of the raw and water-washed rice husk samples	206
Table 4-28:	Diffractiongrams of ash samples from the combustion of raw and water-washed rice husk in the 210-mm inner diameter fluidised bed combustor (effect of alkali metals removal on combustion efficiency in the primary stage) (sand	

	size = 250 – 595 μm , static bed height = 0.5 D_c , fluidising velocity $\approx 3 U_{mf}$, primary air factor ≈ 1.2)	207
Table 4-29:	Ash samples from the combustion of raw and water-washed rice husk in the 210-mm inner diameter fluidised bed combustor (effect of alkali metals removal on combustion efficiency in the primary stage) (sand size = 250 – 595 μm , static bed height = 0.5 D_c , fluidising velocity $\approx 3 U_{mf}$, primary air factor ≈ 1.2)	208
Table 4-30:	Silica structures of ash samples from the combustion of raw and water-washed rice husk in the 210-mm inner diameter fluidised bed (effect of alkali metals removal on combustion efficiency in the secondary stage) (sand size = 250 – 595 μm , static bed height = 0.5 D_c , fluidising velocity ≈ 3 U_{mf} , primary air factor ≈ 1.2 , oxygen level in cyclone = 6 – 12 vol%)	213
Table 4-31:	Ash samples from the combustion of raw and water-washed rice husk in the 210-mm inner diameter fluidised bed (effect of alkali metals removal on combustion efficiency in the secondary stage) (sand size = 250 – 595 μm , static bed height = 0.5 D_c , fluidising velocity $\approx 3 U_{mf}$, primary air factor ≈ 1.2 , oxygen level in cyclone = 6 – 12 vol%)	215
Table 4-32:	Comparisons of ash samples before and after loss on ignition tests (ash from combustion of raw rice husk in the 210-mm inner diameter fluidised bed at different freeboard temperatures; sand size = 250 – 595 μm , static bed height = 0.5 D_c , fluidising velocity $\approx 3 U_{mf}$, primary air factor ≈ 1.2 , oxygen level in cyclone = 6 – 12 vol%)	219

Table 4-33:	Diffraction patterns of fly and bottom ashes from the combustion of rice husk in the 210-mm inner diameter fluidised bed at different primary air factors (sand size = 250 – 595 μm , static bed height = 0.5 D_c , fluidising velocity = 5 – 6 U_{mf})	223
Table 4-34:	Ash samples from the combustion of rice husk in the 210-mm inner diameter fluidised bed at different primary air factors (sand size = 250 – 595 μm , static bed height = 0.5 D_c , fluidising velocity = 5 – 6 U_{mf})	226
Table 4-35:	Ash samples from the combustion of rice husk in the 210-mm inner diameter fluidised bed at different primary-to-secondary air ratios (sand size = 250 – 595 μm , static bed height = 0.5 D_c , fluidising velocity = 5.7 U_{mf} , primary air factor = 0.65)	229
Table 4-36:	Ash samples from the combustion of rice husk in the 210-mm inner diameter fluidised bed combustor at different primary-to-secondary air ratios (sand size = 250 – 595 μm , static bed height = 0.5 D_c , fluidising velocity = 5.7 U_{mf} , primary air factor = 0.65)	231
Table 4-37:	Diffraction patterns of fly ash samples from the combustion of rice husk in the 210-mm inner diameter fluidised bed at different pneumatic air feeding velocities (sand size = 250 – 595 μm , static bed height = 0.5 D_c , fluidising velocity \approx 3 U_{mf} , primary air factor \approx 1.5)	236
Table 4-38:	Fly ash samples from the combustion of rice husk in the 210-mm inner diameter fluidised bed at different pneumatic air feeding velocities (sand size = 250 – 595 μm , static bed height = 0.5 D_c , fluidising velocity \approx 3 U_{mf} , primary air factor \approx 1.5)	240

Table 4-39:	Rice husk samples used for the combustion of water-washed rice husk at different moisture contents in the 210-mm inner diameter fluidised bed combustor	241
Table 4-40:	Diffractiongrams of ash samples from the combustion of water-washed rice husk at different moisture contents in the 210-mm inner diameter fluidised bed combustor (sand size = 250 – 595 μm , static bed height = 0.5 D_c , fluidising velocity $\approx 3 U_{mf}$, primary air factor ≈ 1.2)	243
Table 4-41:	Ash samples from the combustion of water-washed rice husk at different moisture contents in the 210-mm inner diameter fluidised bed combustor (sand size = 250 – 595 μm , static bed height = 0.5 D_c , fluidising velocity $\approx 3 U_{mf}$, primary air factor ≈ 1.2)	245
Table 4-42:	Heat capacities of materials used in the experimental study	252
Table 4-43:	Comparisons of silica structures of ash samples from the combustion of rice husk in the 210-mm inner diameter fluidised bed with different feeding methods (sand size = 250 – 595 μm , static bed height = 0.5 D_c , fluidising velocity $\approx 3 U_{mf}$, primary air factor ≈ 1.2)	254
Table 4-44:	Ash samples from the combustion of rice husk in the 210-mm inner diameter fluidised bed with different feeding methods (sand size = 250 – 595 μm , static bed height = 0.5 D_c , fluidising velocity $\approx 3 U_{mf}$, primary air factor ≈ 1.2)	257
Table 4-45:	Comparisons of physical appearances of different particles from the combustion of rice husk in fluidised bed combustor	258
Table 4-46:	Expected trajectories of particles in the computational fluid dynamics (CFD) model of rice	

	husk combustion in the 210-mm inner diameter fluidised bed combustor with different feeding methods	262
Table 4-47:	Diffraction patterns of ash samples from the combustion of rice husk in the 210-mm inner diameter fluidised bed with inclined, tangential feeding port at different fluidising velocities (sand size = 250 – 595 μm , static bed height = 0.5 D_c , primary air factor ≈ 1.2)	266
Table 4-48:	Ash samples from the combustion of rice husk in the 210-mm inner diameter fluidised bed with inclined, tangential feeding port at different fluidising velocities (sand size = 250 – 595 μm , static bed height = 0.5 D_c , primary air factor ≈ 1.2)	268
Table 5-1:	Trajectories and mass loss history of burning rice husk particles with different sizes in the fluidised bed combustor model ($\varnothing 500\text{mm} \times 5250\text{mm}$)	281
Table 5-2:	Histograms for residence time distribution from computational fluid dynamics (CFD) modelling of burning rice husk particles in the 210-mm inner diameter fluidised bed combustor	286
Table 5-3:	Trajectories and residence times of burning rice husk particles in the 210-mm inner diameter fluidised bed combustor from CFD modelling	287
Table 5-4:	Computational fluid dynamics (CFD) modelling results on the trajectories and residence times of particles during the combustion of rice husk in the 210-mm inner diameter fluidised bed combustor with inclined feeding port (Model FM-A)	295
Table 5-5:	Computational fluid dynamics (CFD) modelling results on the trajectories and residence times of particles during the combustion of rice husk in the	

	210-mm inner diameter fluidised bed combustor with inclined, tangential feeding port (Model FM-B)	296
Table 5-6:	Trajectories and residence times of fly ash particles in Model FM-A (inclined feeding method)	299
Table 5-7:	Trajectories and residence times of fly ash particles in Model FM-B (inclined, tangential feeding method)	300
Table 5-8:	Trajectories of fly ash particles in Model FM-B (inclined, tangential feeding) when the tangential feeding velocity was reduced by half (from 1.1 m/s to 0.55 m/s)	301
Table 5-9:	Mass loss history of burning rice husk particles in Model FM-A (inclined feeding method)	303
Table 5-10:	Mass loss history of burning rice husk particles in Model FM-B (inclined, tangential feeding method)	304
Table 5-11:	Trajectories and residence times of bottom ash particles in Model FM-A (inclined feeding method)	306
Table 5-12:	Trajectories and residence times of bottom ash particles in Model FM-B (inclined, tangential feeding method)	307

LIST OF FIGURES

FIGURE	TITLE	PAGE
Figure 1-1:	Power generation potential from rice husk mills	8
Figure 2-1:	Diffraction pattern of fresh rice husk (taken from Liou, 2004)	40
Figure 2-2:	Diffraction pattern of crystallised rice husk ash showing characteristic crystal peak of cristobalite at 2θ angle of 21.93° (rice husk sample fired at 1000°C at different time intervals) (Ibrahim and Helmy, 1981)	41
Figure 2-3:	Effect of secondary airflow on the temperature distribution in the firebrick-insulated fluidised bed combustor during the combustion of rice husk (Chen et al., 1998)	59
Figure 2-4:	Chart for transport disengaging height (TDH) estimation of fine particle (Geldart A) beds (Zenz and Weil, 1958)	63
Figure 3-1:	Adiabatic flame temperatures from combustion of rice husk sample at different air factors computed using the FLAME programme code	69
Figure 3-2:	Particle size distribution of silica sand samples used in the experimental study	70
Figure 3-3:	Bed particles used in the combustion of rice husk in fluidised bed	71
Figure 3-4:	Boat-like shape of whole rice husk	71
Figure 3-5:	Diffraction pattern of fresh rice husk sample	72

Figure 3-6:	Diffraction pattern of amorphous rice husk ash (from thermal treatment of rice husk in muffle furnace at 600°C and 1 hour)	73
Figure 3-7:	Diffraction pattern of crystallised rice husk ash (exposure to temperature of 725°C for 10 hours in a muffle furnace)	73
Figure 3-8:	Diffraction pattern of fresh silica sand	74
Figure 3-9:	Diffraction pattern of used silica sand (from fluidised bed after combustion of rice husk)	74
Figure 3-10:	Experimental setup of the 80-mm inner diameter Perspex fluidised bed for investigation of fluidisation and mixing behaviours of rice husk	77
Figure 3-11:	Behavioural changes of bed with gas velocity in a conventional fluidised bed (Howard, 1989)	78
Figure 3-12:	Pressure drop versus gas velocity plot for increasing and decreasing gas flow	79
Figure 3-13:	Determination of terminal velocity from the plot of pressure drop versus fluidisation velocity (Hao et al., 1995)	79
Figure 3-14:	Positions of thermocouples (T1 – T6), feeding port and viewing port at the 210-mm inner diameter fluidised bed combustor	86
Figure 3-15:	Overall schematic diagram of the 210-mm inner diameter fluidised bed combustor system	87
Figure 3-16:	Algorithm for the solution of a non-adiabatic two-mixture-fraction case in pre-PDF and FLUENT	105
Figure 3-17:	Size distribution of elutriated sand particles during the combustion of rice husk in the 210-mm inner diameter fluidised bed (bed sand size 250 – 595 μm)	107
Figure 3-18:	Three-dimensional computational grid of the fluidised bed combustor model	107

Figure 3-19:	Three-dimensional computational grid of the 210-mm inner diameter fluidised bed combustor	109
Figure 3-20:	Three-dimensional computational grid of the 210-mm inner diameter fluidised bed combustor with inclined feeding port (Model FM-A)	111
Figure 3-21:	Three-dimensional computational grid of the 210-mm inner diameter fluidised bed combustor with inclined, tangential feeding port (Model FM-B)	111
Figure 4-1:	Experimental values of velocities range for the fluidising state of rice husk, rice husk char, rice husk ash and sand samples	132
Figure 4-2:	Real-time temperature profiles during combustion of rice husk in the 210-mm inner diameter fluidised bed at $3.3 U_{mf}$	154
Figure 4-3:	Real-time temperature profiles during combustion of rice husk in the 210-mm inner diameter fluidised bed at $2.5 U_{mf}$ and $1.5 U_{mf}$	155
Figure 4-4:	Residual carbon contents in fly ash samples from the combustion of rice husk in the 210-mm inner diameter fluidised bed at different fluidising velocities (sand size = 250 – 595 μm , static bed height = $0.5 D_c$, primary air factor ≈ 1.0)	159
Figure 4-5:	Estimated bubble size just before eruption at the bed surface and bubble rise velocity at different static bed heights in the 210-mm inner diameter fluidised bed combustor (sand size = 250 – 595 μm , fluidising velocity = $3 U_{mf}$)	165
Figure 4-6:	Real-time temperature profiles during the combustion of rice husk in the 210-mm inner diameter fluidised bed combustor with sand static bed height of $0.25 D_c$ (sand size = 250 – 595 μm , fluidising velocity $\approx 3 U_{mf}$, primary air factor ≈ 1.0)	167

- Figure 4-7: Real-time temperature profiles during the combustion of rice husk in the 210-mm inner diameter fluidised bed combustor with sand static bed height of $0.5 D_c$ (sand size = $250 - 595 \mu\text{m}$, fluidising velocity $\approx 3 U_{mf}$, primary air factor ≈ 1.0) 169
- Figure 4-8: Real-time temperature profiles during the combustion of rice husk in the 210-mm inner diameter fluidised bed combustor with sand static bed heights of $0.625 D_c$ and $0.75 D_c$ (sand size = $250 - 595 \mu\text{m}$, fluidising velocity $\approx 3 U_{mf}$, primary air factor ≈ 1.0) 171
- Figure 4-9: Temperature profiles during the combustion of rice husk in the 210-mm inner diameter fluidised bed combustor at different static bed heights (sand size = $250 - 595 \mu\text{m}$, fluidising velocity $\approx 3 U_{mf}$, primary air factor ≈ 1.0) 171
- Figure 4-10: Effect of static bed height on the bed temperature and residual carbon content in fly ash during combustion of rice husk in the 210-mm inner diameter fluidised bed combustor (sand size = $250 - 595 \mu\text{m}$, fluidising velocity $\approx 3 U_{mf}$, primary air factor ≈ 1.0) 175
- Figure 4-11: Residual carbon contents in ash samples from the combustion of rice husk in the 80-mm inner diameter fluidised bed at different bed temperatures (sand size = $250 - 595 \mu\text{m}$, fluidising velocity $\approx 4 U_{mf}$, primary air factor ≈ 1.0) 181
- Figure 4-12: Exact locations of thermocouples and secondary burners at the 210-mm inner diameter fluidised bed combustor column 182
- Figure 4-13: Statistical analysis on the bed temperatures (T_1) during combustion of rice husk in the 210-mm inner diameter fluidised bed at different freeboard

- temperatures (sand size = 250 – 595 μm , static bed height = 0.5 D_c , fluidising velocity = 4 – 5 U_{mf} , primary air factor \approx 1.0, oxygen level in cyclone \geq 6 vol%) 183
- Figure 4-14: Statistical analysis on the freeboard temperatures (T3 – T6) during combustion of rice husk in the 210-mm inner diameter fluidised bed – Lower freeboard temperature range (400 – 600°C) (sand size = 250 – 595 μm , static bed height = 0.5 D_c , fluidising velocity = 4 – 5 U_{mf} , primary air factor \approx 1.0, oxygen level in cyclone \geq 6 vol%) 185
- Figure 4-15: Statistical analysis on the freeboard temperatures (T3 – T6) during combustion of rice husk in the 210-mm inner diameter fluidised bed – Higher freeboard temperature range (600 – 700°C) (sand size = 250 – 595 μm , static bed height = 0.5 D_c , fluidising velocity = 4 – 5 U_{mf} , primary air factor \approx 1.0, oxygen level in cyclone \geq 6 vol%) 186
- Figure 4-16: Comparisons of residual carbon contents in ash samples from the combustion of rice husk in the 210-mm inner diameter fluidised bed at different freeboard temperatures (sand size = 250 – 595 μm , static bed height = 0.5 D_c , fluidising velocity = 4 – 5 U_{mf} , primary air factor \approx 1.0, oxygen level in cyclone \geq 6 vol%) 190
- Figure 4-17: Real-time temperature profiles during combustion of rice husk in the non-insulated 210-mm inner diameter fluidised bed combustor system (Case Study HL1) (sand size = 250 – 595 μm , static bed height = 0.5 D_c , fluidising velocity \approx 3 U_{mf} , primary air factor \approx 1.5) 194
- Figure 4-18: Real-time temperature profiles during combustion of rice husk in an insulated 210-mm inner diameter

- fluidised bed combustor system (Case Study HL2)
(sand size = 250 – 595 μm , static bed height = 0.5 D_c , fluidising velocity $\approx 3 U_{mf}$, primary air factor ≈ 1.5) 196
- Figure 4-19: Average combustor temperatures during combustion of rice husk in the non-insulated and insulated 210-mm inner diameter fluidised bed combustors (sand size = 250 – 595 μm , static bed height = 0.5 D_c , fluidising velocity $\approx 3 U_{mf}$, primary air factor ≈ 1.5) 198
- Figure 4-20: Fly ash samples from the combustion of rice husk in the non-insulated and insulated 210-mm inner diameter fluidised bed combustors (sand size = 250 – 595 μm , static bed height = 0.5 D_c , fluidising velocity $\approx 3 U_{mf}$, primary air factor ≈ 1.5) 200
- Figure 4-21: Real-time temperature profile during combustion of raw rice husk in the 210-mm inner diameter fluidised bed combustor (sand size = 250 – 595 μm , static bed height = 0.5 D_c , fluidising velocity $\approx 3 U_{mf}$, primary air factor ≈ 1.2 , oxygen level in cyclone = 6 – 12 vol%) 210
- Figure 4-22: Real-time temperature profile during combustion of water-washed rice husk in the 210-mm inner diameter fluidised bed combustor (sand size = 250 – 595 μm , static bed height = 0.5 D_c , fluidising velocity $\approx 3 U_{mf}$, primary air factor ≈ 1.2 , freeboard temperatures (T4 – T6) = 700 – 900°C, oxygen level in cyclone = 6 – 12 vol%) 211
- Figure 4-23: Comparisons of average bed temperatures during combustion of rice husk in the 210-mm inner diameter fluidised bed at different primary air factors (sand size = 250 – 595 μm , static bed height = 0.5 D_c , fluidising velocity = 5 – 6 U_{mf}) 222

- Figure 4-24: Residual carbon contents of ash samples from the combustion of rice husk in the 210-mm inner diameter fluidised bed at different primary air factors (sand size = 250 – 595 μm , static bed height = 0.5 D_c , fluidising velocity = 5 – 6 U_{mf}) 224
- Figure 4-25: Average combustor temperatures during combustion of rice husk in the 210-mm inner diameter fluidised bed at different primary-to-secondary air ratios (sand size = 250 – 595 μm , static bed height = 0.5 D_c , fluidising velocity = 5.7 U_{mf} , primary air factor = 0.65) 227
- Figure 4-26: Temperature profiles during the combustion of rice husk in a non-insulated combustor (Armesto et al., 2002) 228
- Figure 4-27: Temperature profile along the 210-mm inner diameter fluidised bed combustor during combustion of rice husk at different pneumatic air feeding velocities (sand size = 250 – 595 μm , static bed height = 0.5 D_c , fluidising velocity \approx 3 U_{mf} , primary air factor \approx 1.5) 233
- Figure 4-28: Average bed temperatures and residual carbon contents in ash samples from the combustion of rice husk in the 210-mm inner diameter fluidised bed at different pneumatic air feeding velocities (sand size = 250 – 595 μm , static bed height = 0.5 D_c , fluidising velocity \approx 3 U_{mf} , primary air factor \approx 1.5) 238
- Figure 4-29: Total air velocity at the freeboard region of the fluidised bed combustor at different pneumatic air feeding velocities 238
- Figure 4-30: Comparisons of bed temperatures during combustion of water-washed rice husk at different moisture contents in the 210-mm inner diameter

- fluidised bed combustor (sand size = 250 – 595 μm , static bed height = 0.5 D_c , fluidising velocity $\approx 3 U_{mf}$, primary air factor ≈ 1.2) 242
- Figure 4-31: Comparisons of residual carbon contents of ash samples from the combustion of water-washed rice husk at different moisture contents in the 210-mm inner diameter fluidised bed combustor (sand size = 250 – 595 μm , static bed height = 0.5 D_c , fluidising velocity $\approx 3 U_{mf}$, primary air factor ≈ 1.2) 244
- Figure 4-32: Real-time temperature profiles during combustion of rice husk in the 210-mm inner diameter fluidised bed combustor with inclined feeding port (Case Study FM1) (sand size = 250 – 595 μm , static bed height = 0.5 D_c , fluidising velocity $\approx 3 U_{mf}$, primary air factor ≈ 1.2) 248
- Figure 4-33: Real-time temperature profiles during combustion of rice husk in the 210-mm inner diameter fluidised bed combustor with inclined, tangential feeding port (Case Study FM2) (sand size = 250 – 595 μm , static bed height = 0.5 D_c , fluidising velocity $\approx 3 U_{mf}$, primary air factor ≈ 1.2) 249
- Figure 4-34: Average combustor temperatures during combustion of rice husk in the 210-mm inner diameter fluidised bed combustor utilising different feeding methods (sand size = 250 – 595 μm , static bed height = 0.5 D_c , fluidising velocity $\approx 3 U_{mf}$, primary air factor ≈ 1.2) 250
- Figure 4-35: Histogram of particle size distribution for fly ash from the combustion of rice husk in the 210-mm inner diameter fluidised bed combustor with different feeding methods (sand size = 250 – 595 μm , static bed height = 0.5 D_c , fluidising velocity $\approx 3 U_{mf}$, primary air factor ≈ 1.2) 260

- Figure 4-36: Histogram of particle size distribution for bottom ash from the combustion of rice husk in the 210-mm inner diameter fluidised bed combustor with different feeding methods (sand size = 250 – 595 μm , static bed height = 0.5 D_c , fluidising velocity $\approx 3 U_{mf}$, primary air factor ≈ 1.2) 261
- Figure 4-37: Average temperatures in the combustor during combustion of rice husk in the 210-mm inner diameter fluidised bed combustor with inclined, tangential feeding port at different fluidising velocities (sand size = 250 – 595 μm , static bed height = 0.5 D_c , primary air factor ≈ 1.2) 264
- Figure 4-38: Comparisons of residual carbon contents in ash samples from the combustion of rice husk in the 210-mm inner diameter fluidised bed combustor with inclined tangential feeding port at different fluidising velocities (sand size = 250 – 595 μm , static bed height = 0.5 D_c , primary air factor ≈ 1.2) 269
- Figure 4-39: Particle size distribution of fly ash samples from the combustion of rice husk in the 210-mm inner diameter fluidised bed combustor with inclined, tangential feeding at different fluidising velocities (sand size = 250 – 595 μm , static bed height = 0.5 D_c , primary air factor ≈ 1.2) 271
- Figure 4-40: Particle size distribution of bottom ash samples from the combustion of rice husk in the 210-mm inner diameter fluidised bed combustor with inclined, tangential feeding at different fluidising velocities (sand size = 250 – 595 μm , static bed height = 0.5 D_c , primary air factor ≈ 1.2) 272
- Figure 5-1: Trajectory of the 25 μm sand particle in the fluidised bed combustor model ($\varnothing 500\text{mm} \times 5250\text{mm}$) 278

Figure 5-2:	Trajectory of the 50 μm sand particle in the fluidised bed combustor model ($\varnothing 500\text{mm} \times 5250\text{mm}$)	278
Figure 5-3:	Trajectory of the 75 μm sand particle in the fluidised bed combustor model ($\varnothing 500\text{mm} \times 5250\text{mm}$)	279
Figure 5-4:	Trajectory of the 100 μm sand particle in the fluidised bed combustor model ($\varnothing 500\text{mm} \times 5250\text{mm}$)	279
Figure 5-5:	Trajectory of the 125 μm sand particle in the fluidised bed combustor model ($\varnothing 500\text{mm} \times 5250\text{mm}$)	280
Figure 5-6:	Residence time of burning rice husk particles with different sizes in the fluidised bed model ($\varnothing 500\text{mm} \times 5250\text{mm}$)	283
Figure 5-7:	Statistical analysis on the residence time distribution from computational fluid dynamics (CFD) modelling of burning rice husk particles in the 210-mm inner diameter fluidised bed combustor at different pneumatic air feeding velocities	285
Figure 5-8:	Recirculating zone near the feeding port of the combustor in Model IV (pneumatic air feeding velocity = 1.36 m/s)	288
Figure 5-9:	Absence of recirculating zones inside the fluidised bed combustor in Models I, II and III (pneumatic air feeding velocities of 0.42 – 0.85 m/s)	289
Figure 5-10:	Char fraction of a burning rice husk particle in Model III (pneumatic air feeding velocity = 0.85 m/s)	291
Figure 5-11:	Char fraction of a burning rice husk particle in Model IV (pneumatic air feeding velocity = 1.36 m/s)	291

Figure 5-12:	Gas flow profile as indicated by trajectory of tracer particle in the 210-mm inner diameter fluidised bed with inclined feeding port (Model FM-A)	292
Figure 5-13:	Gas flow profile inside in fluidised bed combustor with inclined feeding port (Model FM-A)	293
Figure 5-14:	Gas flow profile as indicated by trajectory of tracer particle in the 210-mm inner diameter fluidised bed with inclined, tangential feeding port (Model FM-B)	293
Figure 5-15:	Comparisons of residence time of fly ash of different sizes in Model FM-A (inclined feeding) and Model FM-B (inclined, tangential feeding)	302

LIST OF PLATES

PLATE	TITLE	PAGE
Plate 3-1:	The 80-mm inner diameter fluidised bed combustor system	82
Plate 3-2:	The 210-mm inner diameter fluidised bed combustor system (shown without insulation material)	88
Plate 4-1:	Ash product from burning raw rice husk inside the muffle furnace (650 – 750°C) after 10 minutes of combustion time	115
Plate 4-2:	Higher flaming times for a group of rice husk particles spread widely apart in the muffle furnace (650 – 750°C)	116
Plate 4-3:	Formation of dead zone at nearly two-third of the sand bed (595 – 841 μm) at fluidising velocity of $3 U_{mf}$	141
Plate 4-4:	Burning of rice husk was restricted to the top of the sand bed (595 – 841 μm) at fluidising velocity of $3 U_{mf}$	141
Plate 4-5:	Rapid accumulation of char and ash in the sand bed (595 – 841 μm) at fluidising velocity of $3 U_{mf}$	142
Plate 4-6:	Suspension burning of rice husk at fluidising velocity of $4 U_{mf}$ (sand size 595 – 841 μm)	143
Plate 4-7:	Suspension burning of rice husk at fluidising velocity of $5 U_{mf}$ (sand size 595 – 841 μm)	143

Plate 4-8:	Good mixing during the combustion of rice husk (sand size 250 – 595 μm) at fluidising velocity of 3 U_{mf}	146
Plate 4-9:	Penetration of rice husk, char and ash into the sand bed during combustion (sand size 250 – 595 μm) at fluidising velocity of 3 U_{mf}	146
Plate 4-10:	Some degree of suspension burning during the combustion of rice husk (sand size 250 – 595 μm) at fluidising velocity of 4 U_{mf}	148
Plate 4-11:	Vigorous bed bubbling with good mixing of char and rice husk in the sand bed during the combustion of rice husk (sand size 250 – 595 μm) at fluidising velocity of 5 U_{mf}	148
Plate 4-12:	Residual bottom ash retained in the bed after the combustion of rice husk (sand size 250 – 595 μm) at fluidising velocity of 5 U_{mf}	149
Plate 4-13:	The inclined feeding port at the 210-mm inner diameter fluidised bed combustor	247
Plate 4-14:	The inclined, tangential feeding port at the 210-mm inner diameter fluidised bed combustor	247

LIST OF SYMBOLS

A	-	Area, (m ²)
Ar	-	Archimedes number $\left(= \frac{\rho_f (\rho_p - \rho_f) g d_m^3}{\mu_f^2} \right)$, (dimensionless)
$C_{1\varepsilon}, C_{2\varepsilon}$	-	Empirical constants, ($C_{1\varepsilon} = 1.42, C_{2\varepsilon} = 1.68$)
C_d, C_g	-	Constants in PDF equations, ($C_d = 2.0, C_g = 2.86$), (dimensionless)
C_D	-	Drag coefficient, (dimensionless)
C_p	-	Heat capacity, [J/(kg • K)]
d_b	-	Bubble size, (m)
d_{bm}	-	Limiting size of bubble expected in a very deep bed, (m)
d_{bo}	-	Initial bubble size, (m)
D_c	-	Column diameter or fluidised bed inner diameter, (m)
d_m	-	Mean particle diameter, (m)
d_p	-	Particle diameter, (m)
d_{pi}	-	Arithmetic mean diameter of screen apertures, (m)
d_{vs}	-	Volume-surface mean diameter $\left(= \frac{1}{\sum_{i=1}^n (x_i / d_{pi})} \right)$, (m)
f	-	Mixture fraction, (dimensionless)
\bar{f}	-	Time-averaged value of f , (dimensionless)
f'^2	-	Mixture fraction variance, (dimensionless)
f_c	-	Fractional conversion $\left(= \frac{m'}{m_{initial} - m_{final}} \right)$, (dimensionless)

F_D	-	Drag force, (N)
g	-	Gravitational acceleration, (= 9.81 m/s ²)
G_κ	-	Generation of turbulent kinetic energy, (m ² /s ²)
h_c	-	Natural or forced convection coefficient, [W/(m ² • K)]
h_r	-	Radiation heat transfer coefficient, [W/(m ² • K)]
H^*	-	Instantaneous enthalpy, (kJ/kg)
$\Delta\hat{H}_c$	-	Heat of combustion of the fuel at reference temperature of 25°C, (J)
\hat{H}_i	-	Specific enthalpy of the i th component at 25°C, [J/(kg • K)]
H_v	-	Heat of vaporization of water, (J/mol)
k	-	Thermal conductivity, [W/(m • K)]
l	-	Latent heat of vaporisation, (J/kg)
L_e	-	Eddy length scale, (m)
l_{or}	-	Spacing between adjacent holes on a perforated plate, (m)
m	-	Mass, (kg)
m'	-	Instantaneous mass, (kg)
m_i	-	Local mass fraction, (dimensionless)
n	-	Number of mole, (kg-mol)
n_i	-	Mole of the i th component in the feed or product, (kg-mol)
N_{or}	-	Number of orifices on a perforated plate, (dimensionless)
p	-	Partial fraction, (dimensionless)
P	-	Pressure, (N/m ²)
$p(f)$	-	Probability Density Function i.e. fraction of time that the fluctuating variable f takes on a value between f and $f + \Delta f$, (s), (dimensionless)
p_1	-	PDF of f_{fuel} , (dimensionless)
p_2	-	PDF of p_{sec} , (dimensionless)
Q_c	-	Rate of heat absorbed by inlet air, (MJ/min)
Q_{loss}	-	Rate of heat loss through convection and radiation, (MJ/min)
Q_p	-	Rate of heat evolved from the combustion process, assuming complete reaction (MJ/min)
Q_s	-	Heat required for sustaining the combustion process, (MJ)

Q_v	-	Rate of heat consumed to vaporise the moisture content in the feed material, (MJ/min)
r	-	Radius, (m)
R	-	Effects of rapid strain and streamline curvature, (kg/s ⁴)
Re	-	Reynolds number $\left(= \frac{\rho_f U d_p}{\mu_f} \right)$, (dimensionless)
S_m	-	Transfer of mass from reacting particles into gas phase, [kg/(m ³ • s)]
T	-	Temperature, (K)
T_{ad}	-	Adiabatic flame temperature, (K)
t_{cross}	-	Particle eddy crossing time, (s)
T_L	-	Fluid Lagrangian integral time $\left(T_L \approx 0.15 \frac{\kappa}{\varepsilon} \right)$, (s)
u	-	Velocity component or velocity component in x -direction, (m/s)
u'	-	Fluctuating component of u , (m/s)
\bar{u}	-	Instantaneous velocity component, (m/s)
u_i, u_j	-	Time-averaged velocity component
U, U_o	-	Fluidising gas velocity, (m/s)
U_b	-	Bubble rise velocity, (m/s)
U_{mf}	-	Minimum fluidising velocity, (m/s)
$U_{mf,m}$	-	Minimum fluidising velocity of a mixture of bed particles, (m/s)
U_{ms}	-	Minimum spouting velocity, (m/s)
v	-	Velocity component in y -direction, (m/s)
V_m	-	Bubble ejection velocity, (m/s)
w	-	Velocity component in z -direction, (m/s)
x_i	-	Mass fraction of the i -th size range in the particles screen analysis, (dimensionless)
z	-	Height of bed of particles, (m)

Greek Letters

α_ε	-	Inverse effective Prandtl number for turbulent dissipation rate, (dimensionless)
α_κ	-	Inverse effective Prandtl number for turbulent kinetic energy, (dimensionless)
α_s	-	Swirl constant, (dimensionless)
δ	-	Empirical constant, (dimensionless)
ε	-	Turbulent dissipation rate, (m^2/s^3)
ξ	-	Emissivity of the combustor surface, (dimensionless)
ϕ_i	-	Instantaneous species concentration, density or temperature, (kmol/m^3 , kg/m^3 or K)
ϕ_s	-	Particle sphericity, (dimensionless)
\varnothing	-	Inner diameter of fluidised bed column, (m)
ζ	-	Normally distributed random number, (dimensionless)
Ω	-	Swirl angular velocity, (rad/s)
ρ	-	Density, (kg/m^3)
σ_t	-	Constant in PDF equations (= 0.7), (dimensionless)
τ	-	Particle relaxation time (s)
τ_e	-	Characteristic lifetime of the eddy, (s)
τ_i	-	Fraction of time that f spends in the Δf band, (s)
θ	-	Bragg angle in x-ray diffraction analysis, ($^\circ$)
κ	-	Turbulent kinetic energy, (m^2/s^2)
μ	-	Dynamic fluid viscosity, ($\text{kg}/\text{m}\cdot\text{s}$)

Subscripts

a	-	Air
$feed$	-	Feed
$final$	-	Final
$fuel$	-	Fuel
i	-	i-direction or chemical species i

<i>initial</i>	-	Initial
<i>j</i>	-	j-direction or chemical species j
<i>m</i>	-	Mixture
<i>s</i>	-	Sand
<i>sec</i>	-	Secondary fuel
<i>t</i>	-	Turbulent conditions
<i>w</i>	-	Water

Abbreviation

ASEAN	-	Association of South-East Asian Nations
ASTM	-	American Society for Testing Materials
BET	-	Brunauer, Emmett and Teller
CFD	-	Computational Fluid Dynamics
DRW	-	Discrete Random Walk
EC	-	European Commission
FKKKSA	-	Fakulti Kejuruteraan Kimia dan Kejuruteraan Sumber Asli
FSDP	-	Full-Scale Demonstration Project
HHV	-	Higher Heating Value
IARC	-	International Agency for Research on Cancer
ID	-	Internal Diameter
LCD	-	Liquid Crystal Display
LHV	-	Lower Heating Value, (MJ/kg)
LOI	-	Loss on Ignition
LPG	-	Liquefied Petroleum Gas
LPM	-	Litre per Minute
MSW	-	Municipal Solid Waste
NIOSH	-	National Institute for Occupational Safety and Health
NO _x	-	Nitrogen Oxides
PDF	-	Probability Density Function
PMET	-	Pittsburg Mineral & Environmental Tech. Inc.
RHA	-	Rice Husk Ash
RM	-	Ringgit Malaysia
RMS	-	Root Mean Square

SEM	-	Scanning Electron Microscopy
TDH	-	Transport Disengaging Height, (m)
USD	-	United States Dollar (USD 1 = RM 3.80)
UTM	-	Universiti Teknologi Malaysia
XRD	-	X-Ray Diffraction

LIST OF APPENDICES

APPENDIX	TITLE	PAGE
Appendix A:	Estimation of Bubble Eruption Velocity	339
Appendix B:	Determination of Particle Sphericity (ϕ_s)	340
Appendix C:	Properties of Rice Husk for its Definition as the Burning Fuel Particle in CFD Modelling (Input Data to Preprocessor PrePDF)	342
Appendix D:	Chart for Determining Sphericity (ϕ_s) of Particles and Theoretical Equations for Estimating Minimum Fluidising Velocity (U_{mf}) and Terminal Velocity (U_t)	343
Appendix E:	Real-Time Temperature Profiles during Combustion of Rice Husk in the 210-mm Inner Diameter Fluidised Bed at Different Freeboard Temperatures	345
Appendix F:	Real-Time Temperature Profiles during Combustion of Raw and Water-Washed Rice Husk in the 210-mm Inner Diameter Fluidised Bed	347
Appendix G:	Mass Balance to Determine the Amount of Stoichiometric Air for Combustion of Rice Husk	348
Appendix H:	Real-Time Temperature Profiles during Combustion of Rice Husk at Different Pneumatic Air Feeding Velocities	349
Appendix I:	List of Publications	350

CHAPTER 1

INTRODUCTION

1.1 Introduction

The purpose of this research was to produce amorphous silica from rice husk through thermal treatment using the fluidised bed technology. Rice husk ash contains among the highest amount of biogenic silica still in its amorphous form (in the excess of 95 wt% silica, SiO₂) (Kaupp, 1984; Kapur, 1985; James and Rao, 1986) compared to other biomass materials, such as ash from sugarcane bagasse (57 – 73% SiO₂) (Jenkins et al., 1996; Natarajan et al., 1998b; Stephens et al., 2003). In addition, the percentage of ash in rice husk is many times higher (at 13 – 25 wt%, dry basis) (Jenkins et al., 1998; Natarajan et al., 1998b; Armesto et al., 2002) compared to that of sugarcane bagasse (at only 1.9 – 6.8 wt%, dry basis) (Jenkins et al., 1998; Natarajan et al., 1998b; Das et al., 2004). Further, it was reported that such a high percentage of silica is very unusual within nature and that no other plant waste even approaches the amount of silica found in rice husk (Beagle, 1974). The recovery of amorphous silica from rice husk is deemed the most economical source of silica due to the presence of abundant source of rice husk around the country, with annual generation rate of approximately 0.5 million tonnes (in the year 2003, Department of Statistics Malaysia). Rice husk has a high calorific value, which at approximately 13 MJ/kg is sufficient to promote sustainable combustion process, thus reducing the cost of fuel required for the conversion process. This is in contrast with the conventional preparation methods which are either energy-intensive (vapour-phase reaction and thermal decomposition technique) or involves high raw

material costs (alkaline extraction method), all of which result in high production costs.

1.2 Benefits of Research

1.2.1 Amorphous Silica

Silica or silicon dioxide (SiO_2) exists in two forms, amorphous and crystalline. Processing of silica of specific quality results in several types of specialty silicas, such as colloidal silica, fumed silica, fused silica, high-purity ground silica, silica gel and precipitated silica (McDonald, 1991). The global demand for specialty silicas is growing at an annual rate of 3% with revenue generation of more than RM 9.5 billion (USD 2.5 billion) (MineSet Partners LLC, 2004). Currently, the Asia Pacific region is the leading consumer in specialty silica with demand exceeding RM 3 billion (USD 800 million) in 2003 (MineSet Partners LLC, 2004).

Among these specialty silicas, silica in its amorphous form has wider industrial applications (as high-purity ground silica and fumed silica) since crystalline silica is carcinogenic to humans and is categorised as an IARC (International Agency for Research on Cancer) Group 1 agent, whereby its exposure could lead to the risk of silicosis. Amorphous silica is used mainly in specialty coatings, plastics, rubber, electronics, abrasives, refractories and optics (McDonald, 1991). It is also a much sought after raw material for the synthesis of various fine chemicals (sodium silicate, zeolite catalysts, aerogel, very pure silicon, silicon nitride, silicon carbide and magnesium silicide). Since 1997, the world consumption of amorphous silica is estimated to be in the excess of 1 million tonnes per annum valued at approximately RM 4,500 per tonne (Chemlink Pty Ltd., 1997). The price of amorphous silica is highly dependent on its grade (particle size and level of impurities) and could range from RM 440 (USD 120; coarse, impure form) to RM 21,000 (USD 5,500; ultra-fine, highly pure form) (McDonald, 1991). By processing into higher end products such as sodium silicate, its economic value is

further elevated. For example, the production of one tonne of sodium silicate requires approximately 135 kg of amorphous silica as raw material. Thus, one tonne of amorphous silica will produce an equivalent of 7.4 tonnes of sodium silicate, which in turn commands a price of RM 2,100 per tonne (USD 550 per tonne; Chemical Market Reporter, 1999). Sodium silicate is then used for the synthesis of nano-chemicals such as aerogel, with selling price of up to RM 19 million per tonne (USD 500 per 100 g; The Star, 2003).

Conventional methods for preparation of amorphous silica requires the use of high temperature (in the excess of 1500°C) and pressure for extracting silicon in pure form from natural deposits of quartzite rock or quartz sand, such as through the thermal decomposition technique and vapour-phase reaction (Tanner et al., 2000; Wu et al., 2000; Sadasivan et al., 1998, Bogush et al., 1988 and Dielt et al., 1981). Quartz sand is used as the raw material as it is the second most common mineral on earth, therefore making it the most common form of crystalline silica. Another preparation method is the sol-gel process but it involves high raw materials cost (Tomozawa et al., 2001). Such preparation methods results in extremely high production costs, which is subsequently reflected in its high market price.

Rice husk is found to contain amorphous silica in the range of 20 – 25 wt% (Hamad, 1981 – 1982; Hanna et al., 1984; Patel et al., 1987; Nakata et al., 1989; Real et al., 1996; Liou, 2004), which upon thermal degradation yields an ash product with an excess of 95 wt% silica. In addition, rice husk is a form of waste from the rice milling industries and is produced in abundance around the country. The amorphous nature of silica in rice husk makes it extractable at a lower temperature range (Kalapathy et al., 2002) and hence, thermal treatment of rice husk to produce amorphous silica is viewed as a more economical process having the potential to replace the conventional high temperature processes. This is because thermal treatment of rice husk actually produces energy instead of consuming energy. The energy produced could be recovered in the form of heat or electricity.

1.2.2 Rice Husk as Silica Source

The presence of silica in rice husk has been discovered as far back as 1938 (Martin, 1938; Chandrasekhar et al., 2003) while its recovery potential had been realised since 1984 (Kaupp, 1984). It is considered a good source of silica having the potential for large-scale production due to the following reasons:-

a) High Silica Content with Amorphous Characteristic

Rice husk contains silica in the range of 20 – 25 wt% (Real et al., 1996; Patel et al., 1987, Conradt et al., 1992 and Chouhan et al., 2000). The silica (SiO_2) in rice husk exists in the hydrated amorphous form like silica gel. Thermal degradation and pyrolysis of rice husk, followed by combustion of the char, result in a highly porous and amorphous silica particulate mass with a varying percentage of unburnt carbon (Kapur, 1985). Combusted at moderate temperature, the white ash obtained from rice husk contains approximately 92 – 97 wt% amorphous silica (Mishra et al., 1985 and Chakraverty et al., 1988) and some amount of metallic impurities that can be further removed by a simple acid-leaching treatment. Other studies consistently reported that rice husk ash contains very high silica content such as Armesto et al. (2002) (87.7 wt% as SiO_2), Liou (2004) (>90 wt% silica), Kapur (1985) (>95 wt% silica) and Houston (1972) (87 – 97 wt% silica).

b) Abundant and Cheap Source of Silica

Rice is cultivated in more than 75 countries (Natarajan et al., 1998a) and over 97% of rice husk are generated in developing countries (Armesto et al., 2002). Rice husk accounted for 14 – 35 wt% of the paddy harvested, depending on the variety, with an average of 20 wt% (Jenkins, 1989 and Mahin, 1986). Thus, worldwide annual husk output is estimated at 80 million tonnes (Kapur, 1985).

Closer to home, the annual paddy output in Malaysia, up to 2003, was 2.26 million tonnes (Department of Statistics Malaysia) and considering rice husk accounted for 22% of this value, the amount of rice husk generated was approximately 0.5 million tonnes per annum. Rice husk is considered as a form of waste from rice milling processes and are often left to rot slowly in the field or burnt in the open. Although a

small portion of the rice husk is used as a component in animal beddings, the fact that it is a cheap and abundant source of silica remains largely unrealised. To some extent, rice husk has been utilised as fuel for cooking and parboiling of paddy rice in some developing country, but it is neither fully nor efficiently utilised. Such under-utilisation clearly shows the wastage and loss of resources which in reality could generate revenue through the recovery of silica via methods such as combustion.

Kaupp (1984) noted that the ash content of approximately 20 wt% in rice husk (which comprise of over 95 wt% silica) would make rice husk utilisation systems become very economically attractive. According to Kapur (1985), when rice husk is burnt under controlled conditions, the resulting ash is easily the cheapest bulk source of highly reactive silica with a BET (Brunauer, Emmett and Teller method) surface area which can be as high as 80 m²/g or more. Further, since the ash is obtained as a fine powder, it does not require further grinding (James and Rao, 1986) and thus, making it the most economical source of nanoscale silica (Liou, 2004).

c) Quality of Silica Comparable with Other Expensive Sources of Silica

As reviewed by Real et al. (1996), a number of published literatures (such as Mishra et al., 1985; Chakraverty et al., 1988; and James and Rao, 1986) had concluded that rice husk are an excellent source of high-grade amorphous silica. The silica obtained from rice husk ash is a good material for synthesis of very pure silicon (Amick et al., 1980; Amick, 1982 and Hunt et al., 1984), silicon nitride (Real et al., 1996; Yalçın and Sevinç, 2001), silicon carbide (Krishnarao and Subrahmayam, 1995; Gorthy and Pudukottah, 1999) and magnesium silicide (Ghosh et al., 1991). In addition, this silica has been claimed (Amick, 1982; Chakraverty et al., 1985; and Hunt et al., 1984) to be an excellent source of very pure silicon, useful for manufacturing solar cells for photovoltaic power generation and semiconductors. In the manufacture of silicon carbide from rice husk silica, the processing temperature could be lowered to 1500°C due to the high surface area and intimate contact available from carbon and silica in rice husk. This is considered to be less energy-intensive compared to conventional methods using coal and quartz sand in electric furnaces (Hanna et al., 1984), whereby the processing temperatures are in the order of 2500°C. With silica content in the excess of 95 wt%, rice husk ash can also be used as a substitute for silica in cement manufacture. Preliminary study conducted by Ajiwe et al. (2000)

showed that the produced cement had similar standard compared to commercial cement.

d) Disposal Problem

The current practices to dispose of the large quantities of rice husk through open burning or rotting in field are not environmental-friendly. Open burning results in air pollution with the formation of smoke and particulate matters in the form of char and ash. Rotting in field, on the other hand, results in formation of methane (CH₄), which is a potent greenhouse gas. Combustion of biomass such as rice husk can actually reduce the greenhouse effect by converting emissions that would have been methane into the less potent greenhouse gas carbon dioxide. Since CH₄ is some 25 times more potent as a greenhouse gas than carbon dioxide (CO₂), and since the two gases have similar atmospheric residence times, trading off CH₄ emissions for CO₂ emissions from combustion leads to a large net reduction of the greenhouse effect associated with the disposal of rice husk. Rotting in the field leads to a slow decay of the material, with eventual emissions of approximately equal amount of CH₄ and CO₂ from the carbon that is released during the decay (Morris et al., 1991).

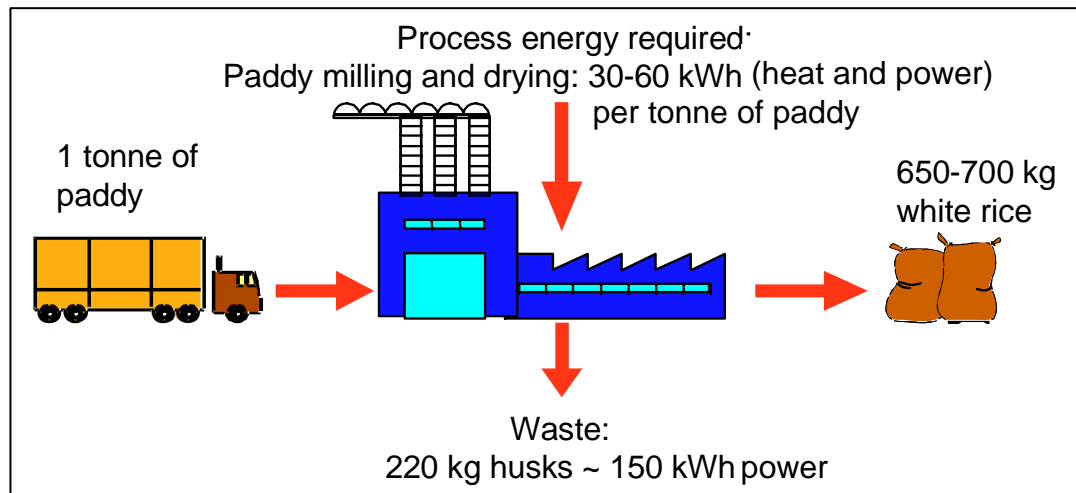
e) High Energy Content

Rice husk has an average lower heating value (LHV) of 13 – 16 MJ/kg (Jenkins, 1989; Mahin, 1986 and Kapur, 1985). Comparisons by Natarajan et al. (1998a) indicated that the LHV of rice husk is about one-third that of furnace oil, one-half that of good quality coal and comparable with sawdust, lignite and peat. It was also reported that the world annual energy potential of rice husk is 1.2×10^9 GJ, with a corresponding heating value of 15 MJ/kg. Thus, rice husk is a good renewable energy source. Apart from solving its disposal problems, combustion offers the potential for energy recovery from this waste.

In Malaysia, with a reported annual generation rate of rice husk at 0.424 million tonnes in the year 2000, the potential energy generation from rice mills is 263 GWh per annum. This translates to a potential capacity of 30 MW (National Energy Balance Malaysia Year 2000 Report). The pressure to search for renewable energy sources is mounting due to the depletion of fossil fuels and the rapid increase in

energy demand, from 25,558 toe (tonne of oil equivalent or equivalent to 42 GJ of lower heating value) in 1998 to 31,515 toe in 2001 (National Energy Balance Malaysia Reports for Year 1998 and 2001). In the Eighth Malaysia Plan (2001 – 2005), the Government replaces the Four-Fuel Diversification Policy with the new Five-Fuel Diversification Policy, which adds renewable energy as a potential source alongside existing four fuels utilised for power generation (oil, gas, coal and hydro). The renewable energy focus is on biomass and the target contribution towards the total electricity generation mix is 5% by 2005 and 10% by 2010. Utilising only 5% of renewable energy could save the country RM5 billion over five years (NSTP, 29th June 2002).

The use of rice husk as renewable energy has already been practised in Malaysia, whereby Bernas and a private rice miller operate a few small (< 1 MW) rice husk cogeneration plants to produce electricity and steam for paddy drying. As shown in Figure 1-1, milling of 1 tonne of paddy produces about 220 kg of rice husk or equivalent to approximately 150 kWh of potential power. In the year 1997, a Full-Scale Demonstration Project (FSDP) under COGEN 3 using rice husk as fuel had been implemented in Ban Heng Bee Rice Mill (1952) Sdn. Bhd. with the commissioning of its 450 kW rice husk-fired cogeneration plant. COGEN 3 is the third phase of the EC-ASEAN cooperation programme initiated by the European Commission (EC) and the Association of South-East Asian Nations (ASEAN). It is financed by the European Commission. COGEN 3 accelerates the implementation of proven, clean and efficient cogeneration projects using biomass, coal or gas as fuel. The projects are implemented through partnerships between ASEAN industrial companies and European equipment suppliers.



Source: EC-ASEAN COGEN Programme

Figure 1-1: Power generation potential from rice husk mills

1.2.3 Market Review for Amorphous Silica from Rice Husk Ash

Currently, the two major commercial applications for amorphous silica from rice husk ash (RHA) are as pozzolan in the cement industry and for manufacture of sodium silicate in the fine chemicals industry. It can also be used in the steel industry as insulator during the steel casting process. However, since it will transform into crystalline form at the end of the steel making process due to prolonged heating at high temperatures (i.e. 1500°C for 4 hours), it is more economically-feasible to use crystalline rice husk ash for such purpose since the price of amorphous ash is higher compared to crystalline ash. The market for crystalline ash (up to 1.0 wt% crystals, carbon content 2.5 – 5.0 wt%) in the steel industry is well-established, with an average price of RM 570 per tonne (USD 150 per tonne) (Bronzeoak, 2003).

a) Cement Industry

Amorphous RHA has been widely researched as mineral cement replacement material (MCRM). The two main research areas for the utilisation of RHA in the cement industry are in the manufacture of low cost building blocks and in the production of high quality cement. Traditionally, silica fume, which is a byproduct

of metallurgical industry, is used for exactly the same purpose but its supply is becoming limited and expensive for developing economies. The current price of silica fume is reported to be RM 4,560 per tonne (USD 1,200 per tonne) in India (Torftech News, 24th November 2003).

Research such as that conducted at FEUP (Faculdade de Engenharia, Universidade do Porto or Faculty of Engineering of University of Porto) in Portugal had shown that RHA concrete performed better than silica fume concrete. Further, studies by Nehdi et al. (2003) showed that depending on the addition rate, RHA increased the compressive strength of concrete by up to 40% at 56 days and was thus deemed superior compared to silica fume. They also concluded that the performance of RHA in reducing the rapid chloride penetrability of concrete was comparable to silica fume and was slightly more efficient than silica fume in resisting surface scaling due to deicing salts. Preliminary studies conducted by Ajiwe et al. (2000) also showed that RHA-formulated cement (RHA substitution of 24.5 wt%, based on the analysis by Bogue (1989) that the theoretical percentage fraction of silica in tricalcium silicate or Portland cement was 26.3 wt%) had similar standard in terms of its compressive strength and setting time compared to commercial cement.

The market of RHA for cement industry is not as well-developed as steel, but there is a great potential due to the pozzolanic properties of RHA that are comparable to cement. The potential is also driven by the absence of any health issues associated with the use of crystalline ash (as in the steel industry) due to the use of amorphous ash. In the United States of America, RHA has already been used commercially by Pittsburg Mineral & Environmental Tech. Inc. (PMET) which is part of Alchemix Corporation, Arizona, as a substitute for silica fume in the production of specialist concrete. PMET specifies that the RHA for use as substitute for silica fume should contain less than 1% of crystalline silica (>99% amorphous), carbon content less than 6% and mean particle size of 7 – 9 μm (passing 45 μm sieve). The current market prices for RHA sold to the cement industry were shown in Table 1-1. The price could reach as high as RM 2,280 per tonne (USD 600 per tonne) for high quality amorphous RHA with more than 85% silica content.

Table 1-1: Market prices for amorphous rice husk ash for use in cement industry

No.	Source/Reference	Price (per tonne)		Remarks
		RM	USD	
1	Torftech Application Description (August 2002)	1,140	300	-
2	The Hindu Newspaper (19 th January 2003)	1,900 – 2,280	500 – 600	Price for super pozzolana (RHA containing high silica content in the excess of 85%)

b) Fine Chemicals Industry

The emerging use of amorphous RHA is for the manufacture of water glass (sodium silicate or Na_2SiO_3), which in turn is an intermediate raw material for synthesis of a wide array of fine chemicals. The current market price for water glass is RM 2,100 per tonne (USD 550 per tonne, Chemical Market Reporter, 18th January 1999).

The conventional process of manufacturing sodium silicate is through the fusion of silica sand with high-purity soda ash in furnaces at high temperatures (1300 – 1500°C), forming water glass (a solid) which is then crushed and dissolved in water and digested under pressure with steam. According to Stephens et al. (2003), the production of water glass through this route formed the foundation of all commercial processes for making sodium or other soluble silicate solutions today. Both the high-temperature fusion and high-temperature and pressure digestion processes are very energy-intensive, thus very expensive. In addition, the silicates produced generally contain metal contaminants found in the earth in amounts ranging from 400 to 10,000 ppm.

The potential for obtaining this expensive sodium silicate solution through the relatively less costly process of caustic digestion of RHA had been reported by Stephens et al. (2003). In their patent (U.S. Patent No. 6,638,354) describing the synthesis of precipitated silicas and silica gels (with and without deposited carbon), the sodium silicate solution required for the synthesis was obtained from digestion of amorphous RHA in a caustic solution of sodium hydroxide. Maintaining the amorphous structure in the RHA is important for its use in the synthesis of chemicals as the silica maintains a porous skeletal structure which provides better chemical reactivity and solubility, especially during operations such as caustic